



# Synthesis and photophysical properties of semiconductor molecules D<sub>1</sub>-A-D<sub>2</sub>-A-D<sub>1</sub>-type structure based on derivatives of quinoxaline and dithienosilole for organics solar cells



M.L. Keshtov<sup>a, \*\*</sup>, D. Yu Godovsky<sup>a</sup>, S.A. Kuklin<sup>a</sup>, A. Nicolaev<sup>a</sup>, J. Lee<sup>b</sup>, B. Lim<sup>b</sup>, H.K. Lee<sup>b</sup>, E.N. Koukaras<sup>c, d</sup>, Ganesh D. Sharma<sup>e, \*</sup>

<sup>a</sup> A.N. Nesmeyanov Institute of Organoelement Compounds, Russian Academy of Sciences, Vavilova Str., 28, Moscow, 119991, Russia

<sup>b</sup> LG Chem Research Park, Daejeon, 104-1, Moonji-dong, Yuseong-gu, 305738, South Korea

<sup>c</sup> Nanotechnology and Advanced Materials Laboratory, Department of Chemical Engineering, University of Patras, Patras, 26500 GR, Greece

<sup>d</sup> Molecular Engineering Laboratory, Department of Physics, University of Patras, Patras, 26500 GR, Greece

<sup>e</sup> Department of Physics, The LNM Institute of Information Technology, Jamdoli, Jaipur, Rajasthan 302031, India

## ARTICLE INFO

### Article history:

Received 1 September 2016

Received in revised form

6 October 2016

Accepted 6 October 2016

### Keywords:

D<sub>1</sub>-A-D<sub>2</sub>-A-D<sub>1</sub> based small molecule

Bulk heterojunction solar cells

Solvent additive

Power conversion efficiency

## ABSTRACT

A novel small molecule with D<sub>1</sub>-A-D<sub>2</sub>-A-D<sub>1</sub> structure denoted as **DTS(QxHT)<sub>2</sub>** based on quinoxaline acceptor and dithienosilole donor units was synthesized and its optical and electrochemical properties were investigated. The thin film of **DTS(QxHT)<sub>2</sub>** showed a broad absorption profile covering the solar spectrum from 350 nm to 780 nm with an optical bandgap of 1.63 eV. The energy levels estimated from the cyclic voltammetry indicate that this small molecule is suitable as donor along with PC<sub>71</sub>BM as acceptor for the fabrication solution processed bulk heterojunction solar cells for efficient exciton dissociation and high open circuit voltage. The organic solar cells based on optimized DTS(QxHT)<sub>2</sub>:2:PC<sub>71</sub>BM active layers processed with chloroform and DIO/CF showed overall power conversion efficiency of 3.16% and 6.30%, respectively. The higher power conversion efficiency of the solar cell based on the DIO/CF processed active layer is attributed to enhanced short circuit photocurrent and fill factor may be related to better phase separation between donor and acceptor in the active layer and more balanced charge transport, induced by the solvent additive. The power conversion efficiency of the organic solar cell was further improved up to 7.81% based on active layer processed with solvent additive, using CuSCN as hole transport layer instead of PEDOT:PSS and mainly attributed to increased fill factor and open circuit voltage due the formation of better Ohmic contact between the active layer and the CuSCN layer.

© 2016 Elsevier B.V. All rights reserved.

## 1. Introduction

In the last decade, organic solar cells (OSCs) have attracted notable attention as renewable energy sources due to their unique advantages such as low cost and large area flexible devices via solution processing technique [1]. The most successful OSCs to date are based on a bulk heterojunction (BHJ) active layer which consists of a donor and acceptor [2]. Significant progress has been made in both material development and device optimization (morphology of active layer and interface engineering), and dramatic

improvement has been achieved in the power conversion efficiency (PCE) from less than 2% in 2008 to over 10% in the past three years, using both conjugated polymers [3] and small molecules [4] with the aid of the synergistic optimization of chemical structure design and device engineering. In comparison to polymer donors, conjugated small molecules possess well defined structure to reduce the structural variation in terms of irregularities, molecular weight and polydispersity [5]. Moreover, small molecules can be more easily designed to meet ideal specifications of good donors for BHJ-OSCs such as strong absorption, suitable highest occupied molecular orbital (HOMO) and lowest unoccupied molecular orbital (LUMO) energy levels, high mobility and solubility [6]. Different strategies can be used to design semiconductor molecules, comprising of (a) formation of conjugated donor-acceptor (D-A) structures for achieving broad absorption in visible and near-infrared ranges [6],

\* Corresponding author.

\*\* Corresponding author.

E-mail addresses: [keshtov@ineos.ac.ru](mailto:keshtov@ineos.ac.ru) (M.L. Keshtov), [gdsarma273@gmail.com](mailto:gdsarma273@gmail.com), [sharmagd\\_in@yahoo.com](mailto:sharmagd_in@yahoo.com) (G.D. Sharma).

and (b) introduction of planar structures to achieve high crystallinity, increasing charge carrier mobility, and as a result, short-circuit current. These concepts have been used by us in the synthesis of a new semiconductor molecule with a D1-A-D2-A-D1 structure, **DTS(QxHT)<sub>2</sub>**, which combines favorable properties of dithienosilole (DTS) as a central donor (D<sub>2</sub>), quinoxaline (Qx) and hexyl-bithiophene units as acceptor (A), and terminal groups (D<sub>1</sub>), respectively. DTS has a simple and planar structure, increasing the  $\pi$ -stacking packing and charge transport. Quinoxaline is a relatively simple and planar acceptor, which contributes to intramolecular charge transfer and reduced bandgap of semiconductor molecules. Two terminal groups of thiophene (D<sub>1</sub>) cover the entire visible range, while alkyl substituents provide compound solubility and its self-organization in solid state. DTS has been widely used as a building block in high efficiency organic solar cells [7]. Quinoxaline-containing D-A copolymers in PSC composition have led to efficiencies exceeding 6% [8]. These results suggest that D-A small molecules based on quinoxaline acceptor and other donor units can be effective semiconductor compounds for producing OSCs with good characteristics. On the other hand, to the best of our knowledge, the small molecule with DTS donor and quinoxaline acceptor has not been explored for OSC applications. In continuation to our research work in designing low bandgap polymers and small molecules, we have designed a small molecule with D1-A-D2-A-D1 with quinoxaline acceptor and dithienosilole donor units with hexyl-bithiophene units as terminal units, denoted as **DTS(QxHT)<sub>2</sub>** and its optical and electrochemical properties were investigated in detail. We have used **DTS(QxHT)<sub>2</sub>** as donor along with PC<sub>71</sub>BM as electron acceptor for the fabrication of the solution processed organic bulk heterojunction solar cells and after the optimization of **DTS(QxHT)<sub>2</sub>** to PC<sub>71</sub>BM weight ratio, the device processed from chloroform solvent showed PCE of 3.16%. The PCE has been raised up to 6.30% when a concentration of 3v% of DIO was added to the host chloroform solution as a solvent additive. Moreover, when PEDOT:PSS is replaced by CuSCN as HTL in combination with DIO/CF processed active layer a further enhancement of all photovoltaic parameters is realized leading to an increase in the PCE to 7.81%.

## 2. Experimental details

Synthesis and characterizations of **DTS(QxHT)<sub>2</sub>** and intermediate compounds are described in the supplementary information.

### 2.1. Device fabrication and characterization

The devices were fabricated on indium tin oxide (ITO) coated glass substrates and cleaned via a route solvent ultrasonic cleaning, subsequently with detergent, de-ionized water, acetone, and isopropyl alcohol in ultrasonic bath for 10 min each. Subsequently, the pre-cleaned ITO coated glass substrates were treated with UV-ozone for 20 min. A poly(3,4-ethylenedioxythiophene):poly(styrenesulfonate) (PEDOT:PSS) solution (Clevious P VP Al 4083, H. C. Stark, Germany) was then spin-coated onto the pre-cleaned ITO coated glass substrates, and then dried by baking in an oven at 110 °C for 15 min to get PEDOT:PSS films with a thickness of ~40 nm. The active layer blend layer was prepared by spin coating the chloroform solution of **DTS(QxHT)<sub>2</sub>** and PC<sub>71</sub>BM (with different weight ratios with concentration 18 mg/mL) on top of the PEDOT:PSS layer and dried to evaporate the residual of solvent completely. The ultra-thin poly[(9,9-bis(30-(*N,N*-dimethylamino)-propyl)-2,7-fluorene)-alt-2,7-(9,9-dioctylfluorene)] (PFN) layer was deposited by spin casting at 2000 rpm for 30 s from a 0.02% (w/v) methanol solution. Then, 90 nm aluminum (Al) was thermally deposited in a vacuum under a pressure of 10–5 Pa as a top electrode and the effective area was measured to be 16 mm<sup>2</sup>. The current-voltage (J-V) characteristics

were measured under AM1.5 solar simulator at 100 mW/cm<sup>2</sup> and data were collected using computer controlled Keithley source meter.

The hole mobilities of the active layers were determined by fitting the dark current to the model of space charge limited current (SCLC) in the hole only device with configuration ITO/PEDOT:PSS/active layer/Au. The active layers were deposited under the same conditions as the corresponding solar cells.

## 3. Results and discussion

### 3.1. Synthesis of **DTS(QxHT)<sub>2</sub>**

Synthetic route to 2,6-bis[2,3-(3'-octyloxyphenyl)-8-(5-hexyl-2,2'-bithiophen-5-yl)quinoxaline-5-yl]-4,4-bis(2-ethylhexyl)-4H-silolo[3,2-a:4,5-a']dithiophene **DTS(QxHT)<sub>2</sub>** (**19**) comprising of 16 stages is shown in Scheme 1. Key "building blocks" - (**8**) [9], (**12**) [9], (**18**) [10] were obtained according to methods described in literature. Cross-coupling of quinoxaline derivative **8** with dithienosilole **18** led to formation of new dibromide **13** with 37% yield. Further reaction of compound **13** with bithiophene derivatives **12** led to formation of the desired compound **DTS(QxHT)<sub>2</sub>** with 65% yield being dark purple solid substance. Composition and structure of intermediate compounds **4**, **6–8**, **10–18** and the desired product **DTS(QxHT)<sub>2</sub>** have been characterized by elemental analysis and <sup>1</sup>H NMR spectroscopy (Fig. 1).

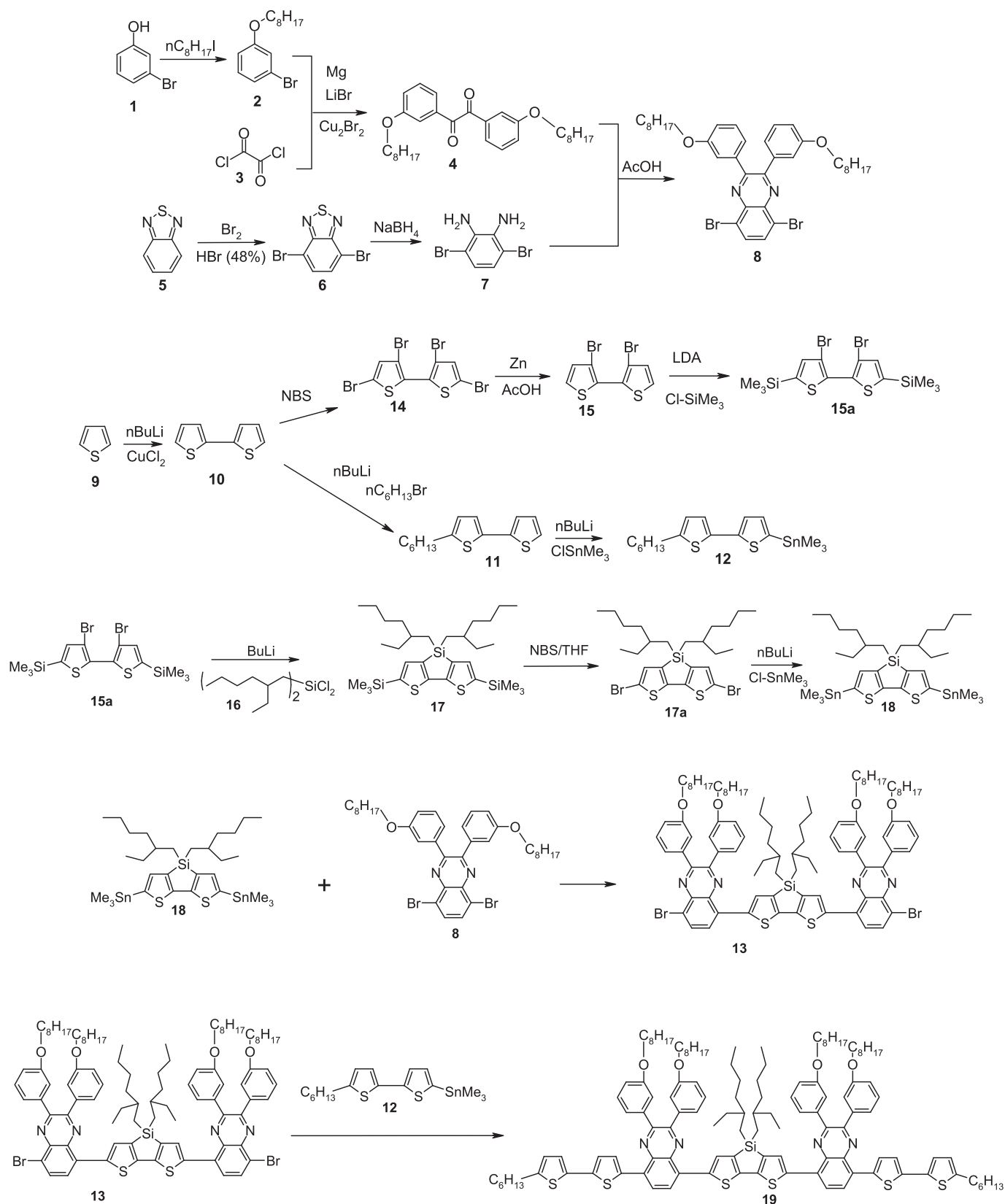
In particular, in the aromatic range of the **DTS(QxHT)<sub>2</sub>** compound proton spectrum at  $\delta$  8.17 ppm there is a broad singlet corresponding to two protons of the quinoxaline fragment; singlet at  $\delta$  7.92 ppm belongs to the hydrogen atom of the dithienosilole cycle. Signals at  $\delta$  7.80, 7.20, 7.12 and 6.75 are doublets belonging to bithiophene terminal fragments. The rest of the signals at  $\delta$  7.6, 7.62, 7.30–7.21 and 7.01–6.95 are protons of octyloxyphenyl substituents. There are two triplets at  $\delta$  3.91 and 4.02 ppm in the aliphatic spectrum range, related to the CH<sub>2</sub> groups directly connected to oxygen atoms. Triplet signal at  $\delta$  2.85 ppm belongs to CH<sub>2</sub> protons of terminal hexyl substituents terminal groups directly bonded with the thiophene fragments. At  $\delta$  1.80–0.75 ppm there are other signals of aliphatic substituents, and the integrated intensity ratio of aliphatic to aromatic fragments is in good consistency with proposed structure of **DTS(QxHT)<sub>2</sub>** small molecule.

### 3.2. Thermal properties

The thermal stability of the **DTS(QxHT)<sub>2</sub>** small molecules was investigated by thermogravimetric analysis (TGA) and decomposition temperatures ( $T_d$  defined as the temperature corresponding 5% mass loss) for **DTS(QxHT)<sub>2</sub>** were determined to be 407 °C (Fig. 2a), indicating high thermal stability of these molecules, adequate for application in organic solar cells. The melting temperatures for **DTS(QxHT)<sub>2</sub>** was determined by differential scanning calorimetry (DSC). In the DSC curves a sharp endothermic peak indicating the melting temperature ( $T_m$ ) is observed for molecule are 126 °C (Fig. 2b).

### 3.3. Optical and electrochemical properties

Fig. 3 shows the normalized absorption spectra of **DTS(QxHT)<sub>2</sub>** in chloroform solution and thin film cast from chloroform solution. In solution **DTS(QxHT)<sub>2</sub>** exhibits broad absorption bands in the shorter wavelength range of 300–450 nm and in the longer wavelength range of 470–720 nm centered at 596 nm, can be assigned to the  $\pi$ - $\pi^*$  transitions in the conjugated chain and intramolecular charge transfer (ICT) in D-A units. In thin film, the absorption profile is broader, and the main ICT absorption band is



**Scheme 1.** Synthetic route of **DTS(QxHT)<sub>2</sub>**.

moved toward a longer wavelength that may be related to better molecules packing and strong inter-chain  $\pi$ - $\pi$  stacking in solid state thus giving rise to electronic delocalization. The optical

bandgap ( $E_g^{opt}$ ) of **DTS(FHT)<sub>2</sub>**, found from the absorption onset of the **DTS(FHT)<sub>2</sub>** absorption spectra, is estimated about 1.63 eV. Wide absorption spectra and narrow optical bandgap for

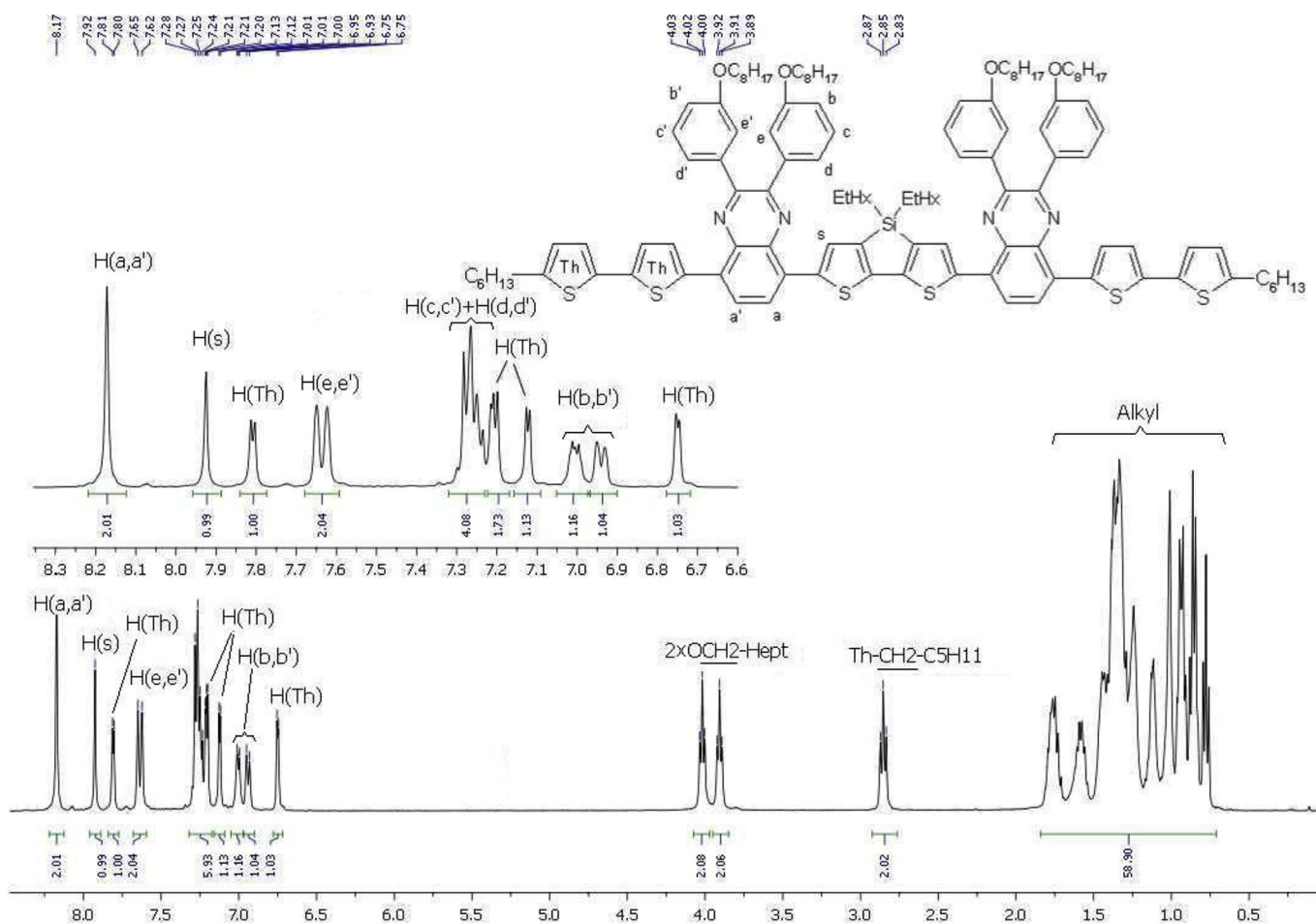


Fig. 1.  $^1\text{H}$  NMR spectra of  $\text{DTS}(\text{QxHT}_2)_2$  small molecule.

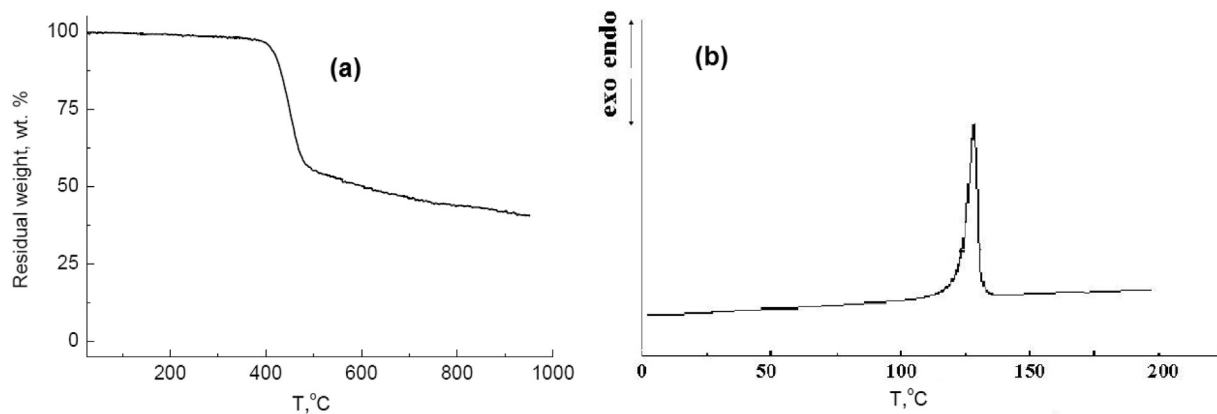


Fig. 2. (a) TGA curves Ar at scan rate 10 deg/min and (b) DSC curves of at scan rate 10 deg/min of  $\text{DTS}(\text{QxHT}_2)_2$ .

$\text{DTS}(\text{FHT}_2)_2$  suggests notable prospects for their application in OSC.

The electrochemical cyclic voltammetry (CV) was performed to measure the HOMO, LUMO energy levels and bandgap ( $E_{\text{g}}^{\text{ec}}$ ) of  $\text{DTS}(\text{QxHT}_2)_2$  (as shown in Fig. 4) and were found to be  $-5.42$ ,  $-3.68$  and  $1.74$  eV, respectively, which are close to values of ideal materials [11] for BHJ-OSCs. The deeper HOMO favors high open-circuit voltage and chemical stability of OSCs in air. On the other hand, the difference between the LUMO of  $\text{DTS}(\text{QxHT}_2)_2$  and the LUMO of (PC<sub>71</sub>BM) is greater than 0.3 eV, which is sufficient for efficient

exciton dissociation in OSC [12]. The higher electrochemical bandgap than optical bandgap may be attributed to the electron transfer for the oxidation and reduction needs to overcome the energy barrier at the electrode/solution interface [13].

#### 3.4. Theoretical calculations

Furthermore, we have performed a theoretical study on the  $\text{DTS}(\text{QxHT}_2)_2$  molecular structure within the framework of density

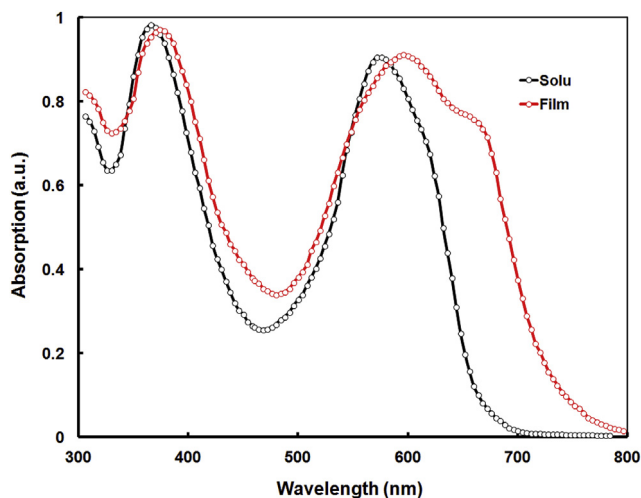


Fig. 3. The normalized absorption spectrum of the compound  $\text{DTS}(\text{QxHT}_2)_2$  in chloroform solution and thin film cast from chloroform solution.

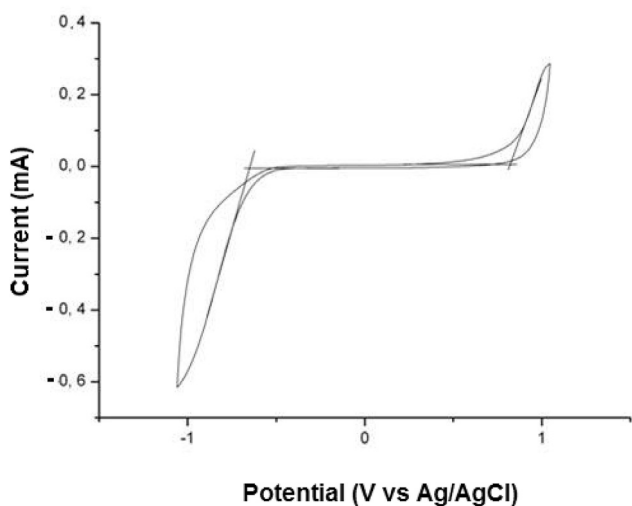


Fig. 4. Cyclic voltammograms of  $\text{DTS}(\text{QxHT}_2)_2$  compounds in acetonitrile 0.1M  $\text{Bu}_4\text{NClO}_4$  at scanning rate  $100 \text{ mV}^{-1}$ .

functional theory (DFT) and time-dependent density functional theory (TD-DFT) [14–18]. Details on the computations are given in the Supplementary Information.

TD-DFT excited state calculations were performed to calculate the optical gaps of  $\text{DTS}(\text{QxHT}_2)_2$  using the same functionals and basis set on the corresponding ground state structures. The UV/Vis spectra were calculated using the B3LYP [17] and M06 [18] functionals. The M06 meta-hybrid functional was chosen since it provides leveled performance over transition types [21,22]. We provide results using all three functionals, which can additionally be used for comparison with the literature. All of the follow up calculations were performed using the Gaussian package [19]. The first round of geometry optimizations was performed using the Turbomole package [20].

The main body of the structure, that consists of dithienosilole (DTS) and quinoxaline (Qx) moieties, is somewhat planar with dihedral angles between these moieties, as well as the thiophenes, in the range of  $\sim 2^\circ$ – $15^\circ$ , depending on the functional and the presence of solvent. We have calculated the HOMO and LUMO energy levels and the optical gaps, defined here as the energetically

lowest allowed vertical electronic excitation, employing the PBE, M06, and B3LYP functionals. In Table 1, in addition to the frontier orbitals' energy levels, we also provide the optical gap the main contributions to the first excitation as well as the wavelength of the first excitation and of the excitations with the largest oscillator strengths.

The HOMO–LUMO (HL) gap calculated using the hybrid B3LYP functional is notably smaller, by 0.37 eV, than that using the meta-hybrid M06 functional, however, the calculated optical gaps only differ by 0.11 eV. In Table 1 we also provide the character of the first allowed excitations only for contributions larger than 4%. The first excitation, as calculated by each of the functional clearly exhibits a single-configuration character. In Fig. 5, we have plotted the isosurfaces (isovalue = 0.02) of the HOMO and LUMO of  $\text{DTS}(\text{QxHT}_2)_2$ . The HOMO and LUMO both extend over the main body, however the LUMO exhibits an increase contribution from the pyrazine of the Qx moiety as well as from the sulfur atoms of the DTS moiety.

Fig. 6 shows the UV/Visible absorbance spectra the  $\text{DTS}(\text{QxHT}_2)_2$  molecular structure calculated at the TD-DFT/M06 level of theory, both accounting for solvent effects for CF and in gas phase. The computed theoretical spectrum overestimates the wavelengths compared to the experimental spectrum by  $\sim 70 \text{ nm}$  in the long wavelength region, and  $\sim 35 \text{ nm}$  in the shorter wavelength region.

### 3.5. Photovoltaic properties

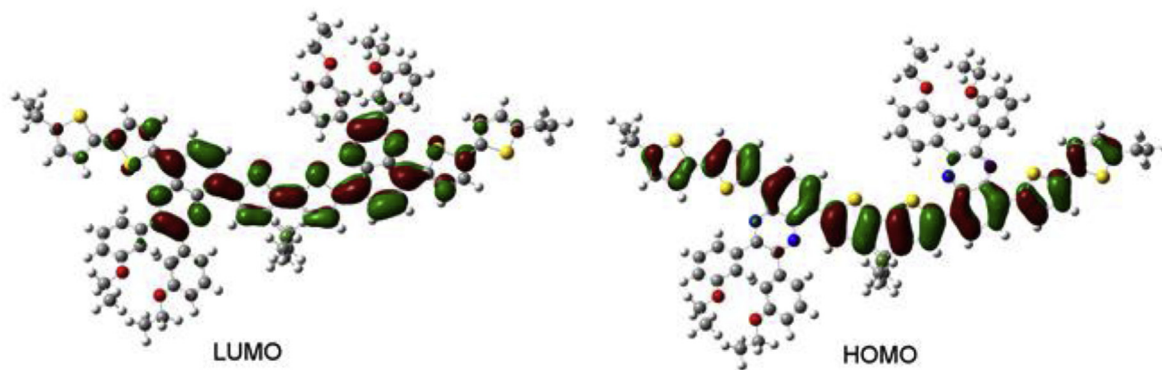
OSC with the device structure ITO/PEDOT:PSS/ $\text{DTS}(\text{QxHT}_2)_2$ :PC<sub>71</sub>BM/PFN/Al were fabricated and characterized to investigate the photovoltaic performance of  $\text{DTS}(\text{QxHT}_2)_2$  as donor in BHJ active layer. First of all, we optimized the D/A weight ratio in chloroform solvent and found that the weight ratio 1:2 showed the best performance. The current–voltage characteristics of the optimized OSCs under AM1.5 G irradiation with  $100 \text{ mW}/\text{cm}^2$  intensity are shown in Fig. 7a and the corresponding photovoltaic parameters are compiled in Table 2. The OSC based on the optimized active layer processed with chloroform showed a PCE of 3.16% with  $J_{\text{sc}}$  of  $7.85 \text{ mA}/\text{cm}^2$ ,  $V_{\text{oc}}$  of 0.96 V and FF of 0.42. The high  $V_{\text{oc}}$  may be related to the deeper HOMO energy level of  $\text{DTS}(\text{QxHT}_2)_2$ , since the  $V_{\text{oc}}$  of OSCs based on BHJ active layer is proportional to the difference of the LUMO level of electron acceptor and HOMO level of the donor. The PCE of the device fabricated with the presence of 3 v% DIO improved up to 6.30% with  $J_{\text{sc}}$  of  $12.08$ ,  $V_{\text{oc}}$  of 0.90 and FF of 0.58. The increase in the PCE has been mainly attributed to the enhancement of both  $J_{\text{sc}}$  and FF, can be contributed by the more ordered molecular self-assembly and better nano-phase separation and D/A networks and therefore more effective charge separation and transportation [23], which is confirmed from the AFM measurements discussed later on. The IPCE spectra of the devices (Fig. 7b) closely resemble the absorption spectra of the corresponding active layers (Fig. 8) and also indicates that both  $\text{DTS}(\text{QxHT}_2)_2$  and PC<sub>71</sub>BM contributes to the exciton generation and thereby photocurrent. Moreover, the IPCE spectra of the optimized device with DIO additive showed a broad response as compared to that of the as cast device, that also confirm the increase in  $J_{\text{sc}}$ . The integration of IPCE spectra yields the estimated  $J_{\text{sc}}$  of  $7.79 \text{ mA}/\text{cm}^2$  and  $11.96 \text{ mA}/\text{cm}^2$  for the as cast and DIO solvent additive based devices, respectively, which are in good agreement with the measured values.

Fig. 8 shows the UV-visible absorption spectra of the blend film cast with and without solvent additive. As shown in Fig. 8 the main ICT absorption peak observed in the as cast blend film is slightly blue shift as compared to the pristine  $\text{DTS}(\text{QxHT}_2)_2$  thin film. However, when the film is processed with DIO, absorption in shorter wavelength region is unchanged but induces a redshift and increased intensity in the longer wavelength region, which can be

**Table 1**  
Calculated properties of  $\text{DTS}(\text{QxHT}_2)_2$ . Specifically, HOMO and LUMO energies (eV), HOMO–LUMO gap (eV), HL, Optical gap (eV), OG, with corresponding oscillator strengths,  $f$ , the wavelengths of the first excitation and excitations with the largest oscillator strengths, the main contributions to the first excited state, and the dipole moment (D),  $\mu$ .

	HOMO (eV)	LUMO (eV)	HL (eV)	OG (eV)	$\lambda_{1\text{st}/\text{max}}$ (nm)	$f$	Main contributions	$\mu$ (D)
$\text{DTS}(\text{QxHT}_2)_2$								
PBE	−4.07	−3.05	1.03	1.28	966	1.26	H → L (96%)	2.77
	−4.29 <sup>a</sup>	−3.26 <sup>a</sup>	1.03 <sup>a</sup>	1.23 <sup>a</sup>	1010 <sup>a</sup>	1.52 <sup>a</sup>	H → L (98%) <sup>a</sup>	3.21 <sup>a</sup>
B3LYP	−4.63	−2.54	2.09	1.79	693/444/428/400/389	1.73	H → L (98%)	2.92
	−4.83 <sup>a</sup>	−2.73 <sup>a</sup>	2.09 <sup>a</sup>	1.73 <sup>a</sup>	715/492/444/426/392 <sup>a</sup>	1.97 <sup>a</sup>	H → L (97%) <sup>a</sup>	3.38 <sup>a</sup>
M06	−4.92	−2.46	2.46	1.90	653/420/405/376/370	1.73	H → L (94%)	2.74
	−5.13 <sup>a</sup>	−2.67 <sup>a</sup>	2.46 <sup>a</sup>	1.84 <sup>a</sup>	674/565/420/404/382 <sup>a</sup>	1.98 <sup>a</sup>	H → L (94%) <sup>a</sup>	3.04 <sup>a</sup>

<sup>a</sup> Values when solvent effects are taken into account for chloroform.



**Fig. 5.** Frontier orbitals i.e. HOMO and LUMO of  $\text{DTS}(\text{QxHT}_2)_2$ .

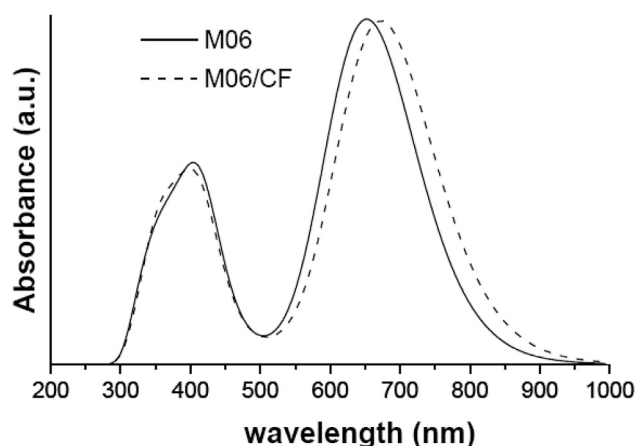


**Fig. 6.** Theoretical UV/Vis absorption spectrum of  $\text{DTS}(\text{QxHT}_2)_2$  (calculated using the M06 functional).

attributed to more ordering of  $\text{DTS}(\text{QxHT}_2)_2$ . This increases the light harvesting efficiency of the device and improves the  $J_{\text{sc}}$  of the device processed with DIO.

In order to get information about the charge transport properties within the active layer processed with different conditions, the space charge limited current (SCLC) was employed to measure the hole and electron mobilities with a device structure ITO/PEDOT:PSS/active layer/Au and ITO/Al/active layer/Al, respectively. The current–voltage characteristics of hole and electron only devices are shown in Fig. 9a,b, respectively. The hole and electron mobilities without additive are about  $4.54 \times 10^{-5} \text{ cm}^2/\text{V}$  and  $2.64 \times 10^{-4} \text{ cm}^2/\text{V}$ , respectively. However, when the active layer is processed with DIO additives, the hole and electron mobilities are increased up to  $1.45 \times 10^{-4} \text{ cm}^2/\text{V}$  and  $2.76 \times 10^{-4} \text{ cm}^2/\text{V}$ ,

respectively, indicating the balanced charge transport in the device, which is consistent with the increase in FF. The electron mobility of the active layer is mainly determined by the n-type  $\text{PC}_{71}\text{BM}$  in the active layer, which show slight increase by DIO additive indicating that the packing behavior of  $\text{PC}_{71}\text{BM}$  may be adjusted by the solvent additive due to the high boiling point of DIO [24] and attributed to the better nanoscale phase separation for electron transport. The increase in hole mobility leads to the decrease in the electron to hole mobility, results a balanced charge transport, after the solvent additive. These effects increase the power conversion efficiency.

To further get information about the performance enhancement upon the DIO additive for active film, transmission electron microscopy (TEM) images of the active layer films processed with and without DIO additive were investigated and shown in Fig. 10. As shown in Fig. 10, the bright and dark regions in the TEM images correspond to the donor and  $\text{PC}_{71}\text{BM}$  rich domains, respectively [25]. The as cast film shows relatively smooth morphology with surface which is not sufficient for the efficient exciton dissociation as well as for charge transport within the active layer and resulted low  $J_{\text{sc}}$  and FF. When the active layer is processed with DIO, the TEM shows fibrous features with a better phase separation, which is favorable for exciton dissociation and charge transport.

In order to get information about the relationship between the PCE and the packing behavior and crystallinity of the active layer of  $\text{DTS}(\text{QxHT}_2)_2$  with the solvent additive, were investigated by X-ray diffraction (XRD) of the thin films processed with and without DIO additives (Fig. 11). Both CF and DIO/CF cast  $\text{DTS}(\text{QxHT}_2)_2:\text{PC}_{71}\text{BM}$  films showed a reflection peak at  $2\theta = 4.58^\circ$  which is corresponds to the d-spacing of  $\text{DTS}(\text{QxHT}_2)_2$ . As compared to the film cast from CF, the reflection intensity of the  $\text{DTS}(\text{QxHT}_2)_2:\text{PC}_{71}\text{BM}$  was significantly enhanced, indicating that the degree of crystallinity of the active layer, particularly  $\text{DTS}(\text{QxHT}_2)_2$  was improved, which is in agreement with the TEM images that the surface morphology was superior and phase separation was improved. The increased

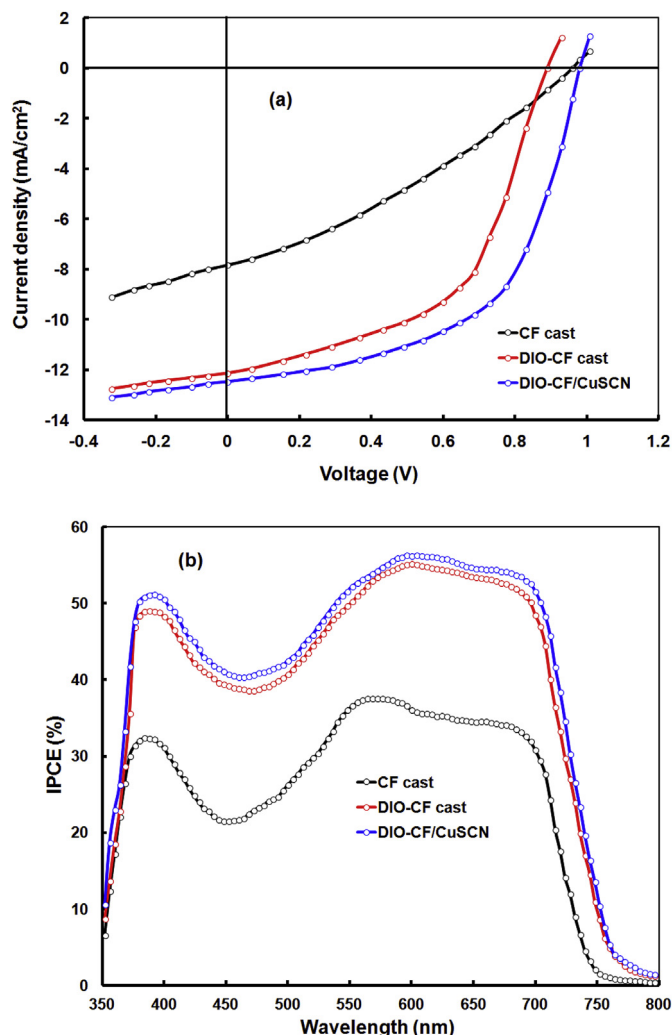


Fig. 7. (a) Current-voltage ( $J$ - $V$ ) characteristics under illumination and (b) IPCE spectra of the organic solar cells based on  $\text{DTS}(\text{QxHT}_2)_2$ :PC71BM active layers processed under different conditions.

**Table 2**  
Photovoltaic parameters of the organic solar cells based on optimized  $\text{DTS}(\text{QxHT}_2)_2$ :PC71BM active layers.

Device	$J_{sc}$ (mA/cm <sup>2</sup> )	$V_{oc}$	FF	PCE (%)	$R_s$ ( $\Omega\text{cm}^{-2}$ )	$R_{sh}$ ( $\Omega\text{cm}^{-2}$ )
CF cast	7.85	0.96	0.42	3.16	13.45	721
DIO/CF cast	12.08	0.90	0.58	6.30	10.74	813
CuNCS/DIO/CF	12.46	0.98	0.64	7.81	10.23	925

crystallinity is beneficial to the charge transport, resulting in an improvement in both  $J_{sc}$  and FF. Moreover, the increase in full width at half maxima (FWHM) of small molecules in the active layer also confirms the increase in the crystalline domain.

In order to get information on the influence of the solvent additives on the electronic properties and light absorption of the devices, the photocurrent density ( $J_{ph}$ ) is plotted against the effective voltage ( $V_{eff}$ ), shown in Fig. 12, and the saturation photocurrent ( $J_{phsat}$ ) and exciton dissociation probabilities ( $P_c$ ) [26] were measured.  $J_{ph}$  is defined as  $J_{ph} = J_L - J_D$ , where  $J_L$  and  $J_D$  are the current densities under illumination and in dark, respectively.  $V_{eff}$  is defined as  $V_{eff} = V_o - V_{appl}$ , where  $V_o$  is the voltage at which  $J_{ph}$  is zero and  $V_{appl}$  is applied voltage. Generally, it is assumed that all the

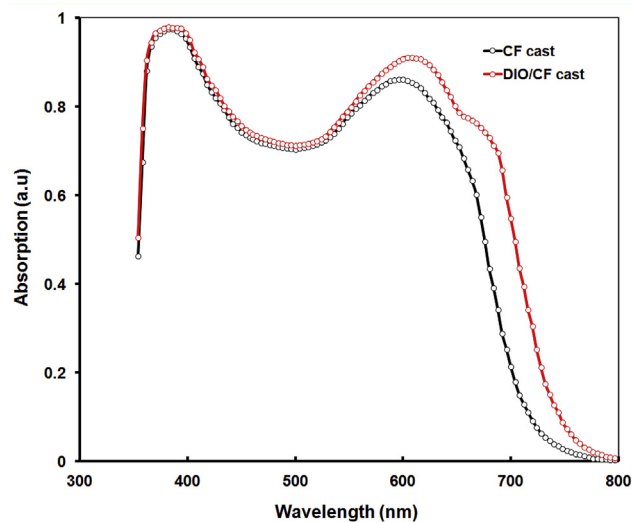


Fig. 8. Normalized absorption spectra of  $\text{DTS}(\text{QxHT}_2)_2$ :PC71BM thin films cast from CF and DIO/CF solutions.

photogenerated excitons are dissociated onto free charge carriers at high  $V_{eff}$ , and  $J_{phsat}$  is only limited by the maximum exciton generation rate ( $G_{max}$ ) and thus  $J_{phsat} = qLG_{max}$ , where  $q$  is the elementary charge and  $L$  is the thickness of active layer.  $G_{max}$  for these devices are as follows:  $7.36 \times 10^{21} \text{ cm}^{-3}/\text{s}$ ,  $9.8 \times 10^{21} \text{ cm}^{-3}/\text{s}$  for the as cast and DIO/CF processed based devices, respectively. The increased value of  $G_{max}$  for the solvent additive based device compared to that of the as cast counterpart suggests an increased overall exciton generation in the device based on the solvent additive processed active layer, which originates from the enhanced absorption in the active layer processed with DIO/CF solvent as indicated by the absorption spectral response (Fig. 8). It should be noted that  $J_{phsat}$  is increased by only 34% with the solvent additive,  $J_{sc}$  increased by 54%, indicating different  $P_c$  for these devices.  $P_c$  is determined as  $P_c = J_{sc}/J_{phsat}$  were 0.74 and 0.83 for the devices fabricated with active layers CF and DIO/CF processed, respectively. This shows that the solvent additive contributed to both light absorption and exciton dissociation in the active layer.

Although the PEDOT:PSS as hole transport layer (HTL), the organic solar cells based on either polymers or small molecules have shown significant improvement in the PCE of these devices. Since the HOMO energy level of  $\text{DTS}(\text{QxHT}_2)_2$  is around  $-5.42 \text{ eV}$ , PEDOT:PSS form a barrier with active layer for hole extraction due to the mismatch of HOMO energy levels [27]. Moreover, the hygroscopic and acidic nature of PEDOT:PSS are the major cause for the long term device stability due to the degradation of the active layer and ITO electrode. Thus, a pH neutral HTL is preferable to avoid the interfacial chemical reactions. It has also been reported that PEDOT:PSS is not a good electron blocking layer and can trap electrons and thus reduce the device performance [28]. In order to overcome the above drawbacks, recently copper thiocyanate (CuSCN) has been used as an efficient solution processable HTL due to its high optical transparency over the visible to near infrared region, high hole mobility ( $0.01\text{--}0.1 \text{ cm}^2 \text{ V}^{-1} \text{ s}^{-1}$ ) and deep valance band edge ( $\sim -5.35 \text{ eV}$ ). We explored the possibility that the overall PCE can be improved using the  $\text{DTS}(\text{QxHT}_2)_2$ :PC71BM active layer by using CuSCN as HTL. As the active layer we have used DIO/CF processed  $\text{DTS}(\text{QxHT}_2)_2$ :PC71BM thin film. The  $J$ - $V$  characteristics of the device are shown in Fig. 7a. The device showed overall PCE of 7.81% with  $J_{sc}$  of  $12.46 \text{ mA}/\text{cm}^2$ ,  $V_{oc}$  of 0.98 V and FF of 0.64 which are higher than that for PEDOT:PSS as HTL. When the CuSCN is used

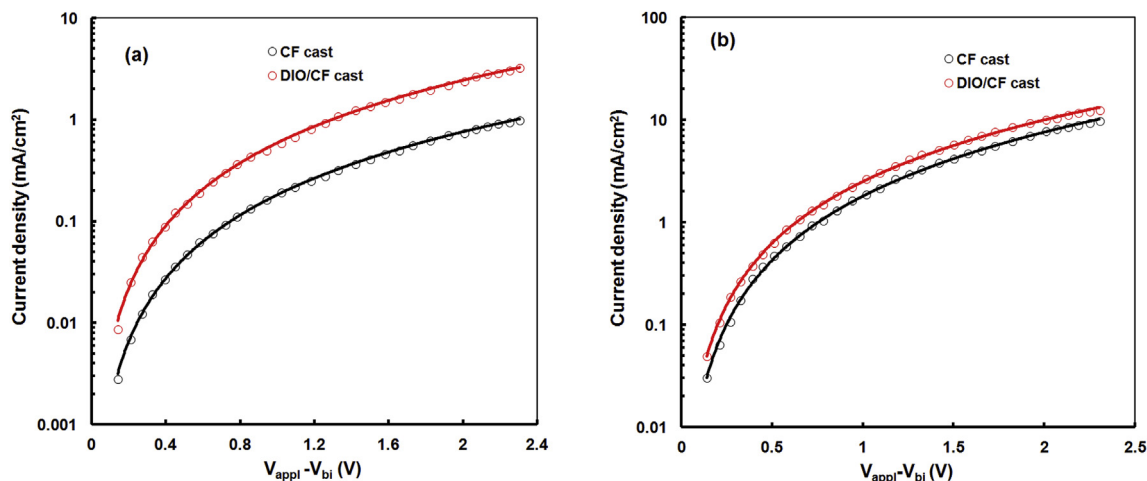


Fig. 9. Dark current-voltage characteristics of (a) hole only and (b) electron only devices based on  $\text{DTS}(\text{QxHT}_2)_2\text{:PC}_{71}\text{BM}$  active layers processed CF and DIO/DF solutions.

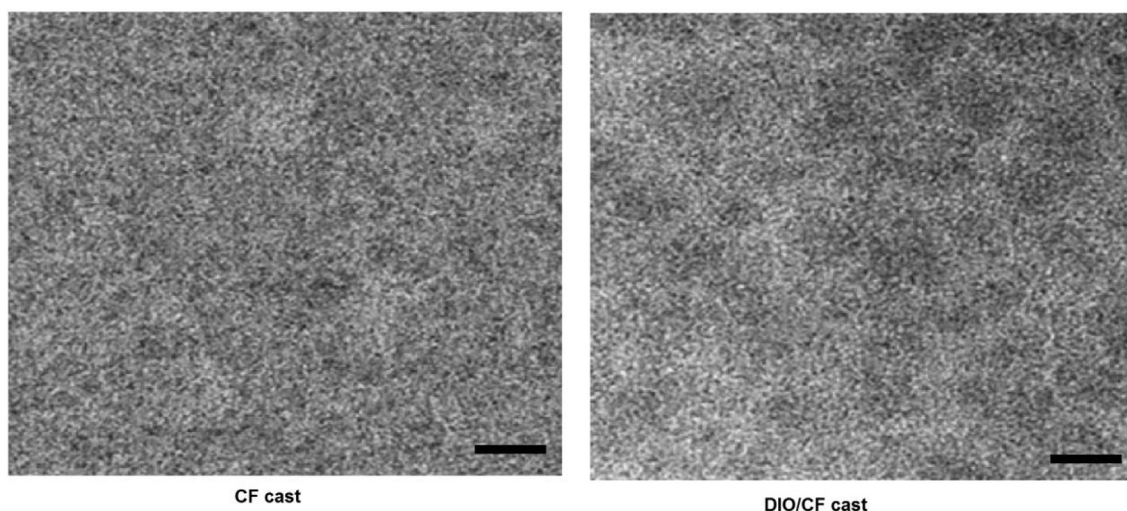


Fig. 10. TEM images of CF and DIO/CF cast  $\text{DTS}(\text{QxHT}_2)_2\text{:PC}_{71}\text{BM}$  films.

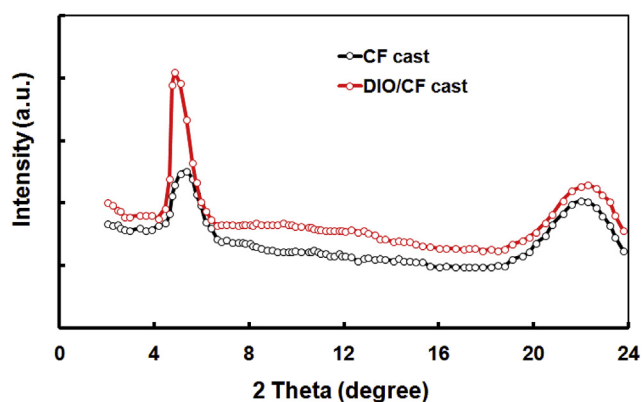


Fig. 11. X-ray diffraction patterns of CF and DIO/CF cast  $\text{DTS}(\text{QxHT}_2)_2\text{:PC}_{71}\text{BM}$  films.

as HTL, the FF has been increased from 0.58 to 0.64, which may be attributed to the better ohmic contact between active layer and CuSCN owing to the valance band edge of CuSCN is deeper than PEDOT:PSS. On the other hand, the increase in the  $V_{oc}$  with CuSCN

relative to PEDOT:PSS could be related to the better alignment between the HOMO level of  $\text{DTS}(\text{QxHT}_2)_2$  ( $-5.42$  eV) with the valance band edge of CuSCN ( $-5.35$  eV) at the active layer/CuSCN interface, which act as electron blocking layer.

Moreover, we estimated the  $P_c$  using the variation of  $J_{ph}$  with  $V_{eff}$  as shown in Fig. 12. As shown in Fig. 12, the value of  $J_{phsat}$  tends to saturate at lower value of  $V_{eff}$  compared to the device based on PEDOT:PSS. The value of  $P_c$  for the device is 0.88, although the value of  $G_{max}$  is about only  $9.7 \times 10^{21}$   $\text{cm}^3/\text{s}$  which is similar to the device based on PEDOT:PSS, indicating the exciton generation rate is almost same for both the devices, since the absorption spectra of PEDOT:PSS and CuSCN are identical. The higher value of  $P_c$  for CuSCN HTL as compared to that for PEDOT:PSS may be due to the formation of better ohmic contact at the active layer/CuSCN interface and holes are extracted more efficiently, leading to a suppression of charge recombination and an increase in FF. As  $V_{eff}$  corresponds to the internal field for extraction of the charge carriers, with low internal field is needed to sweep out the charge carriers. Finally, the estimated series resistance ( $R_s$ ) and shunt resistance ( $R_{sh}$ ) with CuSCN as HTL ( $R_s = 10.23 \Omega\text{cm}^{-2}$  and  $R_{sh} = 10.74 \Omega\text{cm}^{-2}$ ), compared to PEDOT:PSS ( $R_s = 10.74 \Omega\text{cm}^{-2}$  and  $R_{sh} = 813 \Omega\text{cm}^{-2}$ ), also confirm the formation of better ohmic

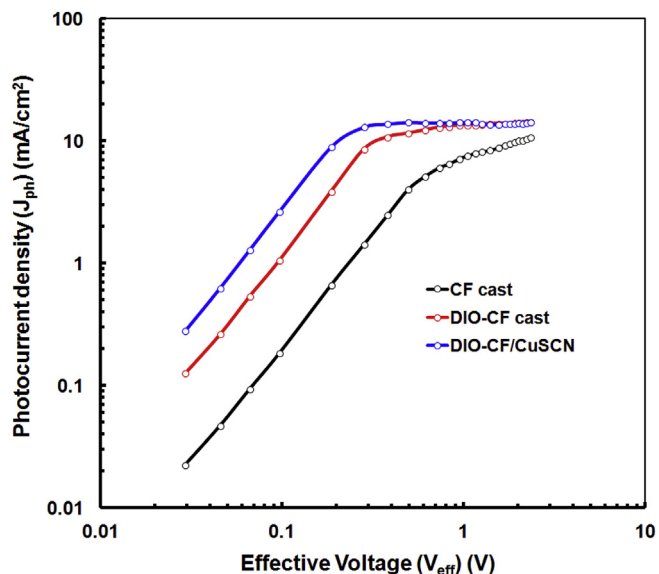


Fig. 12. Variation of photocurrent ( $J_{ph}$ ) with effective voltage ( $V_{eff}$ ) for the organic solar cells processed under different conditions.

contact between active layer and CuSCN HTL.

#### 4. Conclusions

In conclusion, we have developed and characterized optical and electrochemical properties of a novel small molecule with D1-A-D2-A-D1 structure denoted as **DTS(QxHT<sub>2</sub>)<sub>2</sub>** based on quinoxaline acceptor (A) and dithienosilone donor (D2) units and hexyl-bithiophene donor (D1) units as terminal units. The organic solar cells based on optimized **DTS(QxHT<sub>2</sub>)<sub>2</sub>**:PC<sub>71</sub>BM active layers processed with chloroform and DIO/CF showed overall power conversion efficiency of 3.16% and 6.30%, respectively. The enhancement in power conversion efficiency of solar cell based DIO/CF processed active layer is attributed to enhanced short circuit photocurrent and fill factor, may be related to better phase separation between donor and acceptor in the active layer and more balanced charge transport, induced by the solvent additive. The power conversion efficiency of the organic solar cell was further improved up to 7.81% based on active layer processed with solvent additive, using CuSCN as hole transport layer instead of PEDOT:PSS and is mainly attributed to the increased fill factor and open circuit voltage due the formation of better Ohmic contact between the active layer and the CuSCN layer.

#### Acknowledgements

M.L. Keshtov, S.A. Kuklin, D.Y. Godovsky, A.Yu. Nikolaev thank Russian Science Foundation for financial support for experimental research, study of spectral and photovoltaic characteristics (RSF, project 14-13-01444).

#### Appendix A. Supplementary data

Supplementary data related to this article can be found at <http://dx.doi.org/10.1016/j.orgel.2016.10.010>.

#### References

- (a) Y. Liu, J. Zhao, J.Z. Li, C. Mu, W. Ma, H. Hu, K. Jiang, H. Lin, H. Ade, H. Yan, *Nat. Commun.* 5 (2014) 5293–5295;  
(b) T. Xu, L. Yu, *Mater. Today* 17 (2014) 11–15;
- (c) K.A. Mazzi, C.K. Luscombe, *Chem. Soc. Rev.* 44 (2015) 78–90;
- (d) C. Liu, K. Wang, X. Gong, A.J. Heeger, *Chem. Soc. Rev.* 45 (2016) 4825–4846;
- (e) H. Yao, L. Ye, H. Zhang, S. Li, S. Zhang, J. Hou, *Chem. Rev.* 116 (2016) 7397–7457;
- (f) L. Lu, T. Zheng, Q. Wu, A.M. Schneider, D. Zhao, L. Yu, *Chem. Rev.* 115 (2015) 12666–12731.
- G. Yu, J. Gao, J.C. Hummelen, F. Wudl, A.J. Heeger, *Science* 270 (1995) 1789–1791.
- (a) J.D. Chen, C. Cui, Y. Li, L. Zhou, Q.D. Ou, C. Li, Y. Li, J.-X. Tang, *Adv. Mater.* 27 (2015) 1035–1041;  
(b) Y. Liu, J. Zhao, Z. Li, C. Mu, W. Ma, H. Hu, K. Jiang, H. Lin, H. Ade, H. Yan, *Nat. Commun.* 5 (2014) 5293;  
(c) V. Vohra, K. Kawashima, T. Kakara, T. Koganezawa, I. Osaka, K. Takimiya, H. Murata, *Nat. Photonics* 9 (2015) 403–408.
- (a) Y. Liu, C.C. Chen, Z. Hong, J. Gao, T.M. Yang, H. Zhou, L. Dou, G. Li, Y. Yang, *Sci. Rep.* 3 (2013) 3356–3363;  
(b) B. Kan, Q. Zhang, M. Li, X. Wan, W. Ni, G. Long, Y. Wang, X. Yang, H. Feng, Y. Chen, *J. Am. Chem. Soc.* 136 (2014) 15529–15532;  
(c) B. Kan, M. Li, Q. Zhang, F. Liu, X. Wan, Y. Wang, W. Ni, G. Long, X. Yang, H. Feng, *J. Am. Chem. Soc.* 137 (2015) 3886–3893;  
(d) Y. Liu, J. Zhao, Z. Li, C. Mu, W. Ma, H. Hu, K. Jiang, H. Lin, H. Ade, H. Yan, *Nat. Commun.* 5 (2014) 5293;  
(e) Z. He, B. Xiao, F. Liu, H. Wu, Y. Yang, S. Xiao, C. Wang, T.P. Russell, Y. Cao, *Nat. Photonics* 2015 (9) (2015) 174–179.
- (a) A. Mishra, P. Bäuerle, *Angew. Chem. Int. Ed.* 51 (2012) 2020–2067. Y. Li, *Acc. Chem. Res.* 45 (2012) 723–733;  
(b) Y. Chen, X. Wan, G. Long, *Acc. Chem. Res.* 46 (2013) 2645–2655;  
(c) Y. Lin, Y. Li, X. Zhan, *Chem. Soc. Rev.* 2012 (41) (2012) 4245–4272;  
(d) Y. Lin, X. Zhan, *Acc. Chem. Res.* 49 (2016) 175–183.
- (a) M. Li, F. Li, X. Wan, W. Ni, B. Kan, H. Feng, Q. Zhang, X. Yang, Y. Wang, Y. Zhang, Y. Shen, T.P. Russell, Y. Chen, *Adv. Mater.* 27 (2015) 6296–6302;  
(b) N. Lim, N. Cho, S. Paek, C. Kim, J.K. Lee, J. Ko, *Chem. Mater.* 26 (2014) 2283–2288;  
(c) S.C. Lan, P. Raghunath, Y.H. Lu, Y.C. Wang, S.W. Lin, C.M. Liu, J.-M. Jiang, M.C. Lin, K.H. Wei, *ACS Appl. Mater. Interfaces* 6 (2014) 9298–9306.
- (a) Z. Zhang, J. Min, S. Zhang, J. Zhang, Y. Li, *Chem. Commun.* 47 (2011) 9474–9476;  
(b) T.Y. Chu, J. Lu, S. Beaupre, Y. Zhang, J.R. Pouliot, S. Wakim, J. Zhou, M. Leclerc, Z. Li, J. Ding, Y. Tao, *J. Am. Chem. Soc.* 133 (2011) 4250–4253.
- (a) R.M. Duan, L. Ye, X. Guo, Y. Huang, P. Wang, S.Q. Zhang, J.P. Zhang, L.J. Huo, J.H. Hou, *Macromolecules* 45 (2012) 3032–3038;  
(b) Y.J. Zhang, H.L. Zou, K.S. Yip, J.A. Chen, Y.S. Davies, A.K.Y. Jen, *Macromolecules* 44 (2011) 4752–4758.
- H. Wu, B. Qu, Z. Cong, H. Liu, D. Tian, B. Gao, Z. An, C. Gao, L. Xiao, Z. Chen, H. Liu, Q. Gong, W. Wei, *React. Funct. Polym.* 72 (2012) 897–903.
- J. Hou, H. Chen, S. Zhang, G. Li, G.Y. Yang, *J. Am. Chem. Soc.* 130 (2008) 16144–16145.
- H. Zhou, L. Yang, W. You, *Macromolecules* 45 (2012) 607–632.
- C.J. Brabec, C. Winder, N.S. Sariciftci, J.C. Hummelen, A. Dhanabalan, P.A. van Hal, R.A.J. Janssen, *Adv. Funct. Mater.* 12 (2002) 709–712.
- H.J. Son, W. Wang, T. Xu, Y. Liang, Y. Wu, G. Li, L. Yu, *J. Am. Chem. Soc.* 133 (2011) 1885–1894.
- J.P. Perdew, K. Burke, M. Ernzerhof, *Phys. Rev. Lett.* 77 (1996) 3865–3868.
- A. Schafer, H. Horn, R. Ahlrichs, *J. Chem. Phys.* 97 (1992) 2571.
- K. Eichkorn, O. Treutler, H. Öhm, M. Häser, R. Ahlrichs, *Chem. Phys. Lett.* 240 (1995) 283.
- (a) A.D. Becke, *J. Chem. Phys.* 98 (1993) 5648–5652;  
(b) C. Lee, W. Yang, R.G. Parr, *Phys. Rev. B* 37 (1988) 785–789.
- Y. Zhao, D.G. Truhlar, *Theor. Chem. Acc.* 120 (2008) 215–241.
- M.J. Frisch, G.W. Trucks, H.B. Schlegel, G.E. Scuseria, M.A. Robb, J.R. Cheeseman, G. Scalmani, V. Barone, B. Mennucci, G.A. Petersson, H. Nakatsuji, M. Caricato, X. Li, H.P. Hratchian, A.F. Izmaylov, J. Bloino, G. Zheng, J.L. Sonnenberg, M. Hada, M. Ehara, K. Toyota, R. Fukuda, J. Hasegawa, M. Ishida, T. Nakajima, Y. Honda, O. Kitao, H. Nakai, T. Vreven, J.A. Montgomery Jr., J.E. Peralta, F. Ogliaro, M. Bearpark, J.J. Heyd, E. Brothers, K.N. Kudin, V.N. Staroverov, R. Kobayashi, J. Normand, K. Raghavachari, A. Rendell, J.C. Burant, S.S. Iyengar, J. Tomasi, M. Cossi, N. Rega, J.M. Millam, M. Klene, J.E. Knox, J.B. Cross, V. Bakken, C. Adamo, J. Jaramillo, R. Gomperts, R.E. Stratmann, O. Yazyev, A.J. Austin, R. Cammi, C. Pomelli, J.W. Ochterski, R.L. Martin, K. Morokuma, V.G. Zakrzewski, G.A. Voth, P. Salvador, J.J. Dannenberg, S. Dapprich, A.D. Daniels, Ö. Farkas, J.B. Foresman, J.V. Ortiz, J. Cioslowski, D.J. Fox, *Gaussian 03, Revision C.01*, Gaussian, Inc., Wallingford CT, 2004.
- TURBOMOLE (Version 5.6), Universität Karlsruhe, 2000.
- D. Jacquemin, E.A. Perpète, I. Ciofini, Adamo, R. Valero, Y. Zhao, D.G. Truhlar, *J. Chem. Theory Comput.* 6 (2010) 2071–2085.
- S. Mathew, A. Yella, P. Gao, R. Humphry-Baker, F.E. Curchod, N. Ashari-Astani, I. Tavernelli, U. Rothlisberger, M.K. Nazeeruddin, M. Grätzel, *Nat. Chem.* 6 (2014) 242–247.
- (a) H. Qin, L. Li, F. Guo, S. Su, J. Peng, Y. Cao, X. Peng, *Energy Environ. Sci.* 7 (2014) 1397–1401;  
(b) L. Li, L. Xiao, H. Qin, K. Gao, J. Peng, Y. Cao, F. Liu, T.P. Russell, X. Peng, *ACS Appl. Mater. Interfaces* 7 (2015) 21495–21502.
- W. Ni, M. Li, F. Liu, X. Wan, H. Feng, B. Kan, Q. Zhang, H. Zhang, Y. Chen, *Chem.*

- Mater 27 (2015) 6077–6084.
- [25] M.S. Su, C.Y. Kou, M.C. Yuan, U.S. Jeng, C.J. Su, K.H. Wei, *Adv. Mater.* 23 (2011) 3315–3319.
- [26] N. Li, K. Gao, F. Liu, Y. Kan, X. Jiang, L. Liu, Z. Xie, X. Peng, T.P. Russell, Y. Ma, *Adv. Mater.* 28 (2016) 8184–8190.
- [27] D. Poplavskyy, J. Nelson, D.D.C. Bradley, *Appl. Phys. Lett.* 2003 (83) (2003) 707.
- [28] A.W. Hains, J. Liu, A.B.F. Martinsons, M.D. Irwin, T.J. Marks, *Adv. Funct. Mater.* 20 (2010) 595–606.